Author‘s Manuscript - Public Access

Max-Planck-Institut für Polymerforschung
Max Planck Institute for Polymer Research

This is the peer reviewed version of the following article:

Xie, J., Guo, J., Wang, D., Cang, Y., Zhang, W., Zhou, J., et al. (2020). Self-Assembly of Colloidal Nanoparticles into Well-Ordered Centimeter-Long Rods via Crack Engineering. *Advanced Materials Interfaces, 8 (2021)*(2): 2000222. doi:10.1002/admi.202000222.

, which has been published in final form at: 10.1002/admi.202000222

Self-assembly of colloidal nanoparticles into well-ordered centimeter-long rods via crack engineering

Jingli Xie, Junchang Guo, Dehui Wang, Yu Cang, Wenluan Zhang*, Jiajia Zhou, Bo Peng, Yanbo Li, Jiaxi Cui, Longquan Chen, George Fytas and Xu Deng*

This article may be used for non-commercial purposes in accordance with publisher’s Terms and Conditions for Use of Self-Archived Versions

Max Planck Institute for Polymer Research – Author's Manuscript

Self-assembly of colloidal nanoparticles into well-ordered centimeter-long rods via crack engineering

Jingli Xie[1], Junchang Guo[1], Dehui Wang[1], Yu Cang[2], Wenluan Zhang*[3,1], Jiajia Zhou[4], Bo Peng[5], Yanbo Li[1], Jiaxi Cui[1], Longquan Chen[6], George Fytas[2] and Xu Deng*[1]

[1]Institute of Fundamental and Frontier Sciences, University of Electronic Science and Technology of China, Chengdu 610000, China

[2]Max Planck Institute for Polymer Research, Ackermannweg 10, Mainz 55128, China

[3]School of Automation Engineering, University of Electronic Science and Technology of China, Chengdu 610000, China

[4]Center of Soft Matter Physics and Its Application, Beihang University, Beijing 100191, China

[5]National Engineering Research Center of Electromagnetic Radiation Control Materials, University of Electronic Science and Technology of China, Chengdu 610000, China

[6]School of Physics, University of Electronic Science and Technology of China, Chengdu 610000, China

*Corresponding authors. E-mails: dengxu@uestc.edu.cn; wenluanzh@uestc.edu.cn

Tel: 028-83204100

Max Planck Institute for Polymer Research – Author's Manuscript

Abstract

Self-assembly of colloidal nanoparticles (NPs) is widely employed in nano-fabrication to have regulated shape with fascinating functions. However, to have a specific desired shape at centimeter-scale without template is still challenging. Herein, by harnessing the colloidal nanoparticle thin film crack engineering, we are able to obtain robust and highly transparent centimeter-scale rods with uniform width and thickness. The dimension of these rods can be tailored via controlling the solvent composition, NPs volume fraction and suspension descending rate. Their mechanical stiffness and elastic properties can be further improved by thermal annealing. We demonstrate that these rods can be used as probes for Surface enhanced Raman scattering (SERS) detection making use of their rich nanostructured surface. We envision this crack engineering strategy can be used as a universal method to assemble the nano-scale colloids into centimeter-scale rods for analytical and photoelectrical applications.

Keywords: colloidal nanoparticles; cracks; solid-liquid interface; self-assembly; wettability

Introduction

In the field of nano fabrication, to have regulated shape of a large number of colloidal nanoparticles (NPs), self-assembly usually plays an essential role [1]. Through self-assembly, a variety of regulated shapes, e.g. Janus sphere, membrane, strip and rod, which all created from colloidal NPs attract broad interests [2-4]. For example, this nano fabrication strategy can

Max Planck Institute for Polymer Research – Author's Manuscript

be utilized to obtain photonic crystals composed of NPs that respond to mechanical stress like fingerprinting [5]. It can also be employed in forming three-dimensional template to fabricate large inverse opal that exhibits gas adsorption properties [6]. Among all these shapes, colloidal rods (CRs) catch people's eyes in various applications such as photonic devices [7]. battery electrodes [8] and surface patterning [9], etc. However, due to the weak interaction between NPs in the assembling process, the resulted rods are usually in the length scale of micrometer [10-12]. Obtaining CRs in centimeter-long is still challenging. To tackle this issue, the most common method is to use specific template. However, the use of templates requires precise operating conditions and results into high manufacturing cost [13, 14]. Hence, to assemble colloidal NPs into uniform centimeter-scale shape in a facile template-free manner is in great need.

In this work, we report a unique strategy to assemble colloidal NPs into uniform centimeter-scale CRs by harnessing the crack engineering without any templates. Due to tensile stress, cracks are often observed in a wet film where NPs of the suspension self-assemble into some specific shapes via drying. In general, cracks are undesirable and regarded as a negative factor in numerous applications [15-17]. Therefore, most of previous efforts were devoted to circumventing them [15, 18-21]. Recently, it has been demonstrated that regulated crack patterns could be useful in some

Max Planck Institute for Polymer Research – Author's Manuscript

applications, such as fabrication of microchannels [9, 22] and photonic sensors [23], due to their excellent controllability of morphology and periodicity. Herein, we utilized rational designed cracks to obtain uniform CRs. Their dimension can be tailored by adjusting solvent composition, suspension descending rate and NPs volume fraction. The mechanical stiffness of rods is reinforced by annealing without significantly altering the surface nanostructure. Therefore, this strategy is potentially scalable and applicable for different kinds of nanoparticle with multi-functional properties. The resulted CRs' nanostructured surface and the controllable dimension make these CRs appealing for many practical applications.

Materials and Methods

Synthesis and Purification of Silica Nanoparticles

Colloidal suspension containing silica nanoparticles were prepared via a modified Stober method by hydrolysis and condensation of TEOS (Sigma Aldrich) in ethanol (Aladdin), in presence of ammonia (TCI) as catalyst. First, a 250mL flask containing 100mL ethanol and 10mL ammonia were stirred and heated to 60°C. Then 6mL TEOS were added and the mixture is kept under stirring for 8 hours under 60°C. Excess ammonia and unreacted reagents were removed by dialysis in deionized water.

Preparation of Uniform microscale CRs

Glass vials (As-One) containing colloidal suspension were dried in an oven.

Max Planck Institute for Polymer Research – Author's Manuscript

Suspension descending rate was adjusted by changing oven's temperature, ranging from 50 to 100 ℃. Once the suspension surface dropped for 1 cm, residual suspension was taken out and the sample was kept drying to completely remove the solvent. Uniform colloidal rods peeled off by gently shaking the vials.

SERS Detection

For the SERS measurement of the analyte solution, the 10^{-8} M BPA solution was obtained by dissolving the BPA in the ethanol. 10 μL of these probe solution was dropped directly on the tested substrate and allowed to dry prior to measure the spectra. Then, these samples were totally dried for 10 mins. The control substrates were purchased from Suzhou Research Materials Microtech Co., Ltd. All Raman measurements were recorded using a Confocal Raman Microscope, which is coupled with a XY scanning stage (Laser wavelength at 633 nm, 0.52 mW laser power, 10 s acquisition time etc.) These SERS spectra are completely the average spectra randomly collected from at least 3 points on each substrate.

Measurements and Characterizations

The NPs size measurements were performed at a Malvern Zetasizer Nano ZS instrument at 25 ℃. The nanostructures of CRs were observed by field emission scanning electron microscope (FEI, INSPECT F) at an accelerating voltage of 20 kV and atomic force microscope (Bioscope Resolve, Brucker). The transmission was measured by an ultraviolet-

Max Planck Institute for Polymer Research – Author's Manuscript

visible spectrometer (UV-1900, Shimadzu Corporation). The sample for The above transmission measurement is take from Fig1e.

Brillouin Light Spectroscopy (BLS) experiment

The elasticities of CRs were determined by the noninvasive BLS technique. BLS detects the scattering of an incident probing beam from the thermally activated density fluctuations (phonons). The phonon wave vector, $\mathbf{q}=\mathbf{k_i}-\mathbf{k_s}$, is determined by the scattering geometry, where $\mathbf{k_i}$ and $\mathbf{k_s}$ are the incident and scattered photon wave vectors respectively. The scattering wave vector **q** couples to the thermal phonons along the same direction with equal magnitude. The associated phonon energy is represented by the frequency shift $\pm\Delta f$ of inelastically scattered light resolved by an actively stabilized tandem FP interferometer (JRS Instruments). In this work we utilize the transmission geometry to resolve the phonon propagation in the isotropic films. The phonon wave vector $q = 4\pi \sin\left(\frac{\theta}{2}\right)/\lambda$ in this geometry only depends on the scattering angle θ, where λ=532 nm is the wavelength of the probing laser light. The acoustic longitudinal (L) and transverse (T) phonons are selectively recorded in the VV and VH spectra respectively, where VV (VH) denotes a combination of vertical-polarized incident and vertical (horizontal)-polarized scattered light.(Fig.S10) The sound velocities of longitudinal (transverse) phonons are given by $c_{L(T)} = 2\pi\Delta f/q$. Then the elastic moduli E and G can be calculated from $E = \rho(3c_L^2 - 4c_T^2)/(c_L^2 - c_T^2)$ and $G = \rho c_T^2$ where ρ is

Max Planck Institute for Polymer Research – Author's Manuscript

the medium density. The typical VV and VH BLS spectra of CRs annealed for 0.5 h is shown in Fig S10

Results and discussion

We started with radial directional crack pattern. When a droplet of colloidal suspension is dribbled onto a substrate, cracks form and propagate radially inward as solvent evaporates (Fig 1a). The evaporation process is illustrated in Fig S1a. The evolution of crack propagation can be readily observed by means of optical microscopy (Movie S1, Supporting Information). A snapshot of Movie S1 is displayed in Fig S1b, showing a full view of the entire crack pattern after complete evaporation of the solvent. After solvent drying, a rod consisting of colloidal NPs appears between two adjacent cracks. Since the crack propagates into the droplet center, the perimeter of compacting front (CF) becomes small as the solvent evaporates. Thus, the colloidal NPs form smaller rod end near the droplet center than the one away the center[24]. (For detailed illustration, please see Fig S2) To have rods with uniform width, we turned to feather-like crack pattern, which is usually observed during dip coating. While pulling a substrate upward from a colloidal suspension, straight crack pattern appears in the central part of this substrate. The meniscus height in the central part of the substrate, h_1, can be expressed as [25]: $h_1 = \sqrt{2}\kappa^{-1}(1-\sin\theta)^{1/2}$, κ^{-1} is the capillary length and θ is the water contact

Max Planck Institute for Polymer Research – Author's Manuscript

angle. This equation works only if the substrate is flat and the curvature radius is infinite. However, close to the substrate edge, the curvature increases substantially, the meniscus height near the substrate edge, h_2, can be written as [25]: $h_2 \sim b ln(2\kappa^{-1}b^{-1})$, here, curvatures are of the order of b^{-1}. Thus, due to the increased curvature, the meniscus height decreases near the substrate edge and $h_1 > h_2$. This difference in menicus height then leads to curved compacting front. Since the crack propagation direction is vertical to the compacting front, the generated cracks thus bend accordingly, thus rendering curved rods. This phenomenon is illustrated in Fig 1b and S1d [26]. Therefore, to obtain completely straight rods, we used small vial for generating cracks, which has no boundary effect when solvent evaporates along the vertical direction, because the cracks arrange in a close loop at the horizontal level.

Indeed, by adjusting crack patterns, we managed to have uniform centimeter-scale CRs. A vial with colloidal suspension containing 110 nm diameter monodispersed SiO_2 NPs (Fig S3) was placed in an oven with temperature ranging from 50 to 90 ℃. As solvent evaporated, silica NPs accumulated at the three-phase contact line and were adsorbed on the vial's wall. Then, cracks appeared and propagated gradually to form CRs (Fig 1d). After the liquid level decreased by 1 cm, residue suspension was removed and the resulted rods were left alone for half an hour to be completely dried. In this work, we used 10 cm high vials for all the CRs

Max Planck Institute for Polymer Research – Author's Manuscript

fabrication. Hence, the silica NPs volume fraction does not change significantly during the solvent evaporation, so that we were able to obtain 1 cm long CRs with uniform thickness, width and good reproducibility, as shown in Fig 1e, Fig S4. High magnification image from scanning electron microscope (SEM) (Fig 1g) proves that these rods are entirely composed of close-packed silica NPs. In the drying process, solvent evaporation causes NPs aggregate into close-packed structure, binding to the substrate and generating transverse tensile stress [27, 28]. Once the tensile stress exceeds a critical value, cracks occur and propagate along the solvent retreating direction.

In previous works, dip coating was usually applied to construct various colloid patterns, and pure water was used as solvent [23]. However, by evaporating colloidal suspension using water as solvent, we cannot obtain uniform thin film composed of silica NPs, not mentioning CRs. It is possible that, unlike the non-equilibrium dynamic process happens during dip coating, the spontaneous evaporation of water is pretty slow resulting into a quasi-equilibrium state of the colloidal suspension, which cannot confine the NPs aggregation to the vial's wall to form uniform thin film. In practice, we added ethanol into water to enhance the solvent evaporation rate. But this mixture of water and ethanol rendered tears of wine phenomenon, a classic Marangoni effect, with ethanol concentration up to 80 vol%, as shown in Fig S5 and Movie S2 [29, 30]. Small droplets were

Max Planck Institute for Polymer Research – Author's Manuscript

dragged by gravity downwards back to the suspension disrupting the formation of colloidal film. Thus, only small amount of NPs were deposited in the film, which was not thick enough to induce cracks, as shown in Fig S5. When the ethanol concentration higher is than 90 vol%, colloidal film can grow thick and uniform CRs were finally obtained. High concentration ethanol/water suspension was prepared via dialysis, which required ultra-large amount of ethanol to get 99 vol% concentration. In practice, 90 vol% ethanol suspension could render uniform CRs, which was not improved significantly by using 99 vol% ethanol suspension. Thus, we sticked to the 90 vol% ethanol suspension for the rest of the work.

To get desired CRs dimension, like rod thickness (H) and width (W), we studied the effect of silica NPs volume fraction and suspension descending rate. By keeping suspension descending rate 1 μm/s as constant, as shown in Fig 2a, H and W values increase linearly as the NPs volume fraction goes higher, reach about 70 μm and 160 μm respectively. Then, NPs volume fraction of 1.2 vol% was kept unchanged to study how suspension descending rate affected the CRs' dimension. Fig 2b shows that H and W values gradually decrease as the suspension evaporating faster, down to about 30 μm and 70 μm respectively. The W values are in the same trend as the H values, which is in good agreement with previous study [31]. In this case, the suspension descending rate was controlled by heating temperature, obtaining beyond 10 μm/s is simply not possible because it

Max Planck Institute for Polymer Research – Author's Manuscript

would boil the ethanol/water mixture.

To get deeper understanding of the film formation mechanism and its correlated fluid mechanical properties, we propose the CRs formation mechanism in schematic graphs, shown in Fig2c and d, and perform a qualitative analysis. Based on previous study on meniscus guided coating [32, 33], we argue that the film deposition, in this case, is in the so-called "evaporative regime", since the capillarity and evaporation of the solvent dominate the wet film formation, NPs transport and film solidification afterward. Normally, in this regime, dry film thickness is proportional to the suspension descending rate at the power of -1. However, in the inset of Fig 2b, the thickness (H) decreases by a power-law exponent of –0.4, which is larger than -1. Note that the previous power-law dependence of film thickness was derived by mass conservation law and neglecting flow recirculation induced by thermal Marangoni effect. In this study, the suspension descending rate is even lower than the lowest speed of the previous works. It is very possible that Marangoni flow contributes the thicker films as predicted by previous "evaporative regime" model. However, considering the complexity of fluid field, concentration and temperature gradient induced by evaporation, it is still not feasible to give accurate model for the time being. Further investigation is needed in this interesting direction.

The CRs are composed of close-packed 110 nm NPs and the voids

Max Planck Institute for Polymer Research – Author's Manuscript

between NPs are much smaller than the wavelength of visible light, generating a highly transparent film, as verified by the ultraviolet-visible transmittance spectra (Fig 3a). However, these rods constructed by silica NPs are fragile and easily broken into pieces, making it difficult to be transferred. Hence, it is crucial to enhance the mechanical stiffness of the rods for practical application. According to a previous study [34], the mechanical stiffness of the rods can be enhanced through annealing. Hence, we evaluated the effect of annealing temperature on rod morphology ranging from 800 to 1100 ℃ (Fig S8). As the temperature was higher than 1000 ℃, the silica NPs undergo high temperature deformation, resulting in the necking between NPs that gradually fused or fully sintered and the rod morphology changes. Under the premise of not changing the rod morphology, 900 ℃ was chosen as the annealing temperature. Annealing duration, on the other hand, plays an important role in improving the mechanical strength of rods due to the positive correlation between the annealing duration and the interactive force between silica NPs. For the untreated sample with the density of 1.69 kg/cm^3 , the Young's (E) and shear (G) modulus determined by Brillouin light spectroscopy (BLS) [35] are 4.2 GPa and 1.8 GPa, respectively. As the annealing duration increases from 0.5 h to 4 hours, the rod density increases by 5%, from 2.13 to 2.24 kg/cm^3. Both E and G moduli are enhanced by about 250%, from 17.6 to 43.5 GPa, and from 8.2 to 19.1 GPa, respectively (Fig 3b). This extreme

Max Planck Institute for Polymer Research – Author's Manuscript

increase of the elasticity is attributed mainly to the huge packing (density) effect but also to the increased elasticity of the NPs due to size shrinking with annealing (Fig S9). Notably the Poisson's ratio (ν=0.1) of CRs annealed for 0.5h is lower than in the amorphous glass (ν =0.16).

For practical application, these highly uniform nanostructured CRs can be employed as probes for Surface enhanced Raman scattering (SERS) detection. SERS, as a signal amplification and detection technique [36], has shown great potential for imaging and sensing applications [37-39]. Accordingly, a variety of efficient plasmonic nanostructures have been fabricated to achieve the SERS-based signal amplification and detection of trace molecules [40-42]. However, it remains a great challenge to transform the analytical sensitivity of SERS detection into an practical in situ diagnostic probe, mainly from the difficulty to prepare a robust, metal-coated SERS substrate. In this study, we utilized these CRs for SERS as a show case as shown in Fig 4a. Once the CRs were fabricated, they were coated with a thin (30 nm) sliver layer through electron beam evaporation. After the deposition of silver layer, SEM analysis was performed (Fig 4b) to confirm that the origin of the observed SERS effects arose from the nanogap structure. Control substrates were also fabricated using above method where silica rod substrate was replaced by silicon wafers with a 300-nm thick oxide layer, yielding a smooth unpatterned surface. We chose Bisphenol A (BPA) as target molecule, since its broad existance in plastic

Max Planck Institute for Polymer Research – Author's Manuscript

packages, and it is harmful to the endocrine system once released and entered human body. As shown in Fig 4c, SERS spectra of 10^{-8} M BPA adsorbed on these two substrates are recorded with laser excitation source of 633 nm wavelength. The spectra recorded using nanostructured substrate showed an obvious SERS response. The characteristic Raman peaks of BPA at 405, 484, 840, 993, 1140, 1280, 1602 cm^{-1} can be observed. However, no appreciable Raman signal is observed from the control substrate (the blue spectra). Above results strongly support the fact that the nanostructured substrate are densely decorated by Ag, forming 3D plasmonic structure which provides abundant hot spots to have better SERS performance.

Conclusions

In summary, by controlling the stress distribution inside the colloidal film and crack formation during the evaporation of colloidal suspension, we successfully obtained centimeter-scale CRs with highly uniform width and thickness. The dimension of these CRs can be tailored by controlling NPs volume fraction and suspension descending rate. These colloid rods are transparent and the mechanical stiffness can be tuned by thermal annealing. For practical application, these robust rods can be used to fabricate probes in SERS detection. In addition to probes, these robust, regulated rods which could be manufactured in large-scale may have potential values for a wide

Max Planck Institute for Polymer Research – Author's Manuscript

range of applications, including sensors, photonics, lithography.

Conflict of interest

The authors declare that they have no conflict of interest.

Acknowledgments

This work was supported by the National Natural Science Foundation of China (21603026). Y.C and G.F acknowledge the financial support by ERC AdG SmartPhon (Grant No. 694977).

Referances

[1] Vogel N, Retsch M, Fustin CA, et al. Advances in colloidal assembly: The design of structure and hierarchy in two and three dimensions. Chem Rev 2015; 115: 6265-311.
[2] Glotzer SC, Solomon MJ. Anisotropy of building blocks and their assembly into complex structures. Nat Mater 2007; 6: 557-62.
[3] Nisisako T, Torii T, Takahashi T, et al. Synthesis of monodisperse bicolored janus particles with electrical anisotropy using a microfluidic co-flow system. Adv Mater 2006; 18: 1152-+.
[4] Li Q, Jia Y, Dai LR, et al. Controlled rod nanostructured assembly of diphenylalanine and their optical waveguide properties. Acs Nano 2015; 9: 2689-95.
[5] Arsenault AC, Clark TJ, Von Freymann G, et al. From colour fingerprinting to the control of photoluminescence in elastic photonic crystals. Nat Mater 2006; 5: 179-84.
[6] Kang S, Yu JS, Kruk M, et al. Synthesis of an ordered macroporous carbon with 62 nm spherical pores that exhibit unique gas adsorption properties. Chem Commun 2002; 1670-1.
[7] Dong JW, Chen XD, Zhu HY, et al. Valley photonic crystals for control of spin and topology. Nat Mater 2017; 16: 298-+.
[8] Pikul JH, Zhang HG, Cho J, et al. High-power lithium ion microbatteries from interdigitated three-dimensional bicontinuous nanoporous electrodes. Nat Commun 2013; 4: 1732.
[9] Li B, Jiang BB, Han W, et al. Harnessing colloidal crack formation by flow-enabled self-assembly. Angew Chem Int Ed 2017; 56: 4554-9.
[10] Wu GX, Cho H, Wood DA, et al. Confined assemblies of colloidal particles with soft repulsive interactions. J Am Chem Soc 2017; 139: 5095-101.
[11] Jiang LX, de Folter JWJ, Huang JB, et al. Helical colloidal sphere structures through thermo-reversible co-assembly with molecular microtubes. Angew Chem Int Ed 2013; 52: 3364-

Max Planck Institute for Polymer Research – Author's Manuscript

8.
[12] Bharti B, Fameau AL, Rubinstein M, et al. Nanocapillarity-mediated magnetic assembly of nanoparticles into ultraflexible filaments and reconfigurable networks. Nat Mater 2015; 14: 1104-+.
[13] Li F, Badel X, Linnros J, et al. Fabrication of colloidal crystals with tubular-like packings. J Am Chem Soc 2005; 127: 3268-9.
[14] Rozynek Z, Han M, Dutka F, et al. Formation of printable granular and colloidal chains through capillary effects and dielectrophoresis. Nat Commun 2017; 8: 15255.
[15] Russell JL, Noel GH, Warren JM, et al. Binary colloidal crystal films grown by vertical evaporation of silica nanoparticle suspensions. Langmuir 2017; 33: 10366-73.
[16] Harris DJ, Hu H, Conrad JC, et al. Patterning colloidal films via evaporative lithography. Phys Rev Lett 2007; 98: 148301.
[17] Wang B, Weldon AL, Kumnorkaew P, et al. Effect of surface nanotopography on immunoaffinity cell capture in microfluidic devices. Langmuir 2011; 27: 11229-37.
[18] Phillips KR, Shirman T, Shirman E, et al. Nanocrystalline precursors for the co-assembly of crack-free metal oxide inverse opals. Adv Mater 2018; 30: 1706329.
[19] Mishchenko L, Hatton B, Kolle M, et al. Patterning hierarchy in direct and inverse opal crystals. Small 2012; 8: 1904-11.
[20] Hatton B, Mishchenko L, Davis S, et al. Assembly of large-area, highly ordered, crack-free inverse opal films. P Natl Acad Sci USA 2010; 107: 10354-9.
[21] Choi SY, Mamak M, Coombs N, et al. Thermally stable two-dimensional hexagonal mesoporous nanocrystalline anatase, meso-nc-tio2: Bulk and crack-free thin film morphologies. Adv Funct Mater 2004; 14: 335-44.
[22] Han W, Li B, Lin ZQ. Drying-mediated assembly of colloidal nanoparticles into large-scale microchannels. Acs Nano 2013; 7: 6079-85.
[23] Dalstein O, Gkaniatsou E, Sicard C, et al. Evaporation-directed crack-patterning of metal-organic framework colloidal films and their application as photonic sensors. Angew Chem Int Ed 2017; 56: 14011-5.
[24] Jing GY, Ma J. Formation of circular crack pattern in deposition self-assembled by drying nanoparticle suspension. J Phys Chem B 2012; 116: 6225-31.
[25] De Gennes P-G, Brochard-Wyart F, Quéré D. Capillarity and wetting phenomena: Drops, bubbles, pearls, waves. Springer Science & Business Media, 2013
[26] Huang JX, Kim F, Tao AR, et al. Spontaneous formation of nanoparticle stripe patterns through dewetting. Nat Mater 2005; 4: 896-900.
[27] Tirumkudulu MS, Russel WB. Cracking in drying latex films. Langmuir 2005; 21: 4938-48.
[28] Lee WP, Routh AF. Why do drying films crack? Langmuir 2004; 20: 9885-8.
[29] Velarde MG. Drops, liquid layers and the marangoni effect. Philos T R Soc A 1998; 356: 829-43.
[30] Fournier JB, Cazabat AM. Tears of wine. Europhys Lett 1992; 20: 517-22.
[31] Smith MI, Sharp JS. Effects of substrate constraint on crack pattern formation in thin films of colloidal polystyrene particles. Langmuir 2011; 27: 8009-17.
[32] Gu XD, Shaw L, Gu K, et al. The meniscus-guided deposition of semiconducting polymers. Nat Commun 2018; 9:
[33] Faustini M, Louis B, Albouy PA, et al. Preparation of sol-gel films by dip-coating in extreme

Max Planck Institute for Polymer Research – Author's Manuscript

conditions. J Phys Chem C 2010; 114: 7637-45.
[34] Widiyastuti W, Lee SY, Iskandar F, et al. Sintering behavior of spherical aggregated nanoparticles prepared by spraying colloidal precursor in a heated flow. Adv Powder Technol 2009; 20: 318-26.
[35] Kearns KL, Still T, Fytas G, et al. High-modulus organic glasses prepared by physical vapor deposition. Advanced Materials 2010; 22: 39-+.
[36] Kneipp K, Wang Y, Kneipp H, et al. Single molecule detection using surface-enhanced raman scattering (sers). Phys Rev Lett 1997; 78: 1667-70.
[37] Nie SM, Emery SR. Probing single molecules and single nanoparticles by surface-enhanced raman scattering. Science 1997; 275: 1102-6.
[38] Xu HX, Bjerneld EJ, Kall M, et al. Spectroscopy of single hemoglobin molecules by surface enhanced raman scattering. Phys Rev Lett 1999; 83: 4357-60.
[39] Lim DK, Jeon KS, Kim HM, et al. Nanogap-engineerable raman-active nanodumbbells for single-molecule detection. Nat Mater 2010; 9: 60-7.
[40] Fang Y. Measurement of the distribution of site enhancements in surface-enhanced raman scattering (vol 321, pg 388, 2008). Science 2008; 322: 1790-.
[41] Zhu CH, Meng GW, Zheng P, et al. A hierarchically ordered array of silver-nanorod bundles for surface-enhanced raman scattering detection of phenolic pollutants. Advanced Materials 2016; 28: 4871-6.
[42] Le F, Brandl DW, Urzhumov YA, et al. Metallic nanoparticle arrays: A common substrate for both surface-enhanced raman scattering and surface-enhanced infrared absorption. Acs Nano 2008; 2: 707-18.

Max Planck Institute for Polymer Research – Author's Manuscript

Figure 1. Strategy designed for uniform crack-induced CRs. a) Illustration of radial-directional crack pattern by sessile drop evaporation. The white line and arrows represent the compacting front and the evaporation direction, respectively. b) Illustration of feather-like crack pattern through dip-coating. c) Illustration of the meniscus on the substrate, h represents the meniscus height and $h_1 > h_2$. d) Schematic drawing illustrating the preparation of the CRs. e) An optical image of crack-induced rods. f, g) SEM images of CRs at different magnification.

Max Planck Institute for Polymer Research – Author's Manuscript

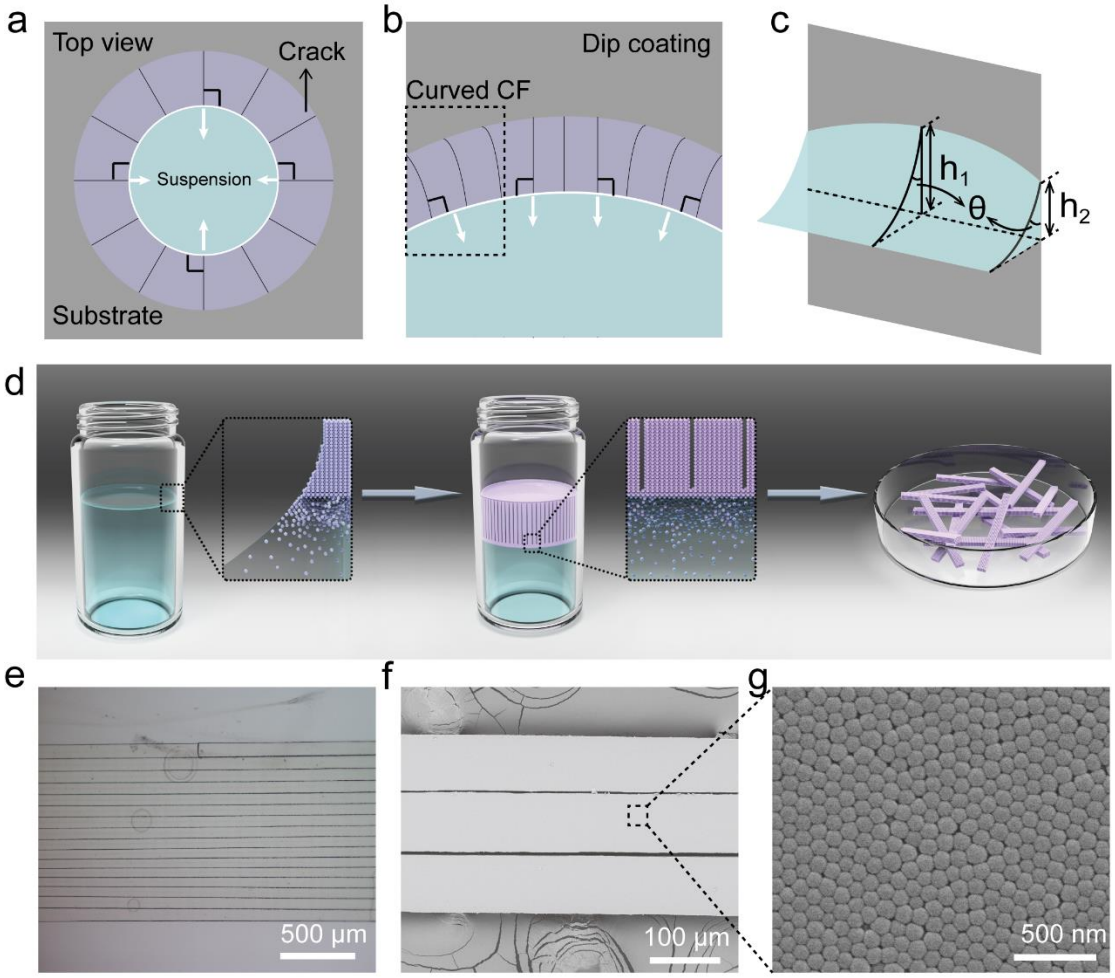

Figure 2. Experimental results of CRs dimension. a) Rods' width and thickness as a function of NPs volume fraction. b) The dependence of both rods width and thickness on the suspension descending rate. The inset is plotted in log-log scale. c) Flow pattern sketch of the drying suspension near the contact line. d) Schematic illustrating crack propagation during the deposition of NPs leading to the formation of rods.

Max Planck Institute for Polymer Research – Author's Manuscript

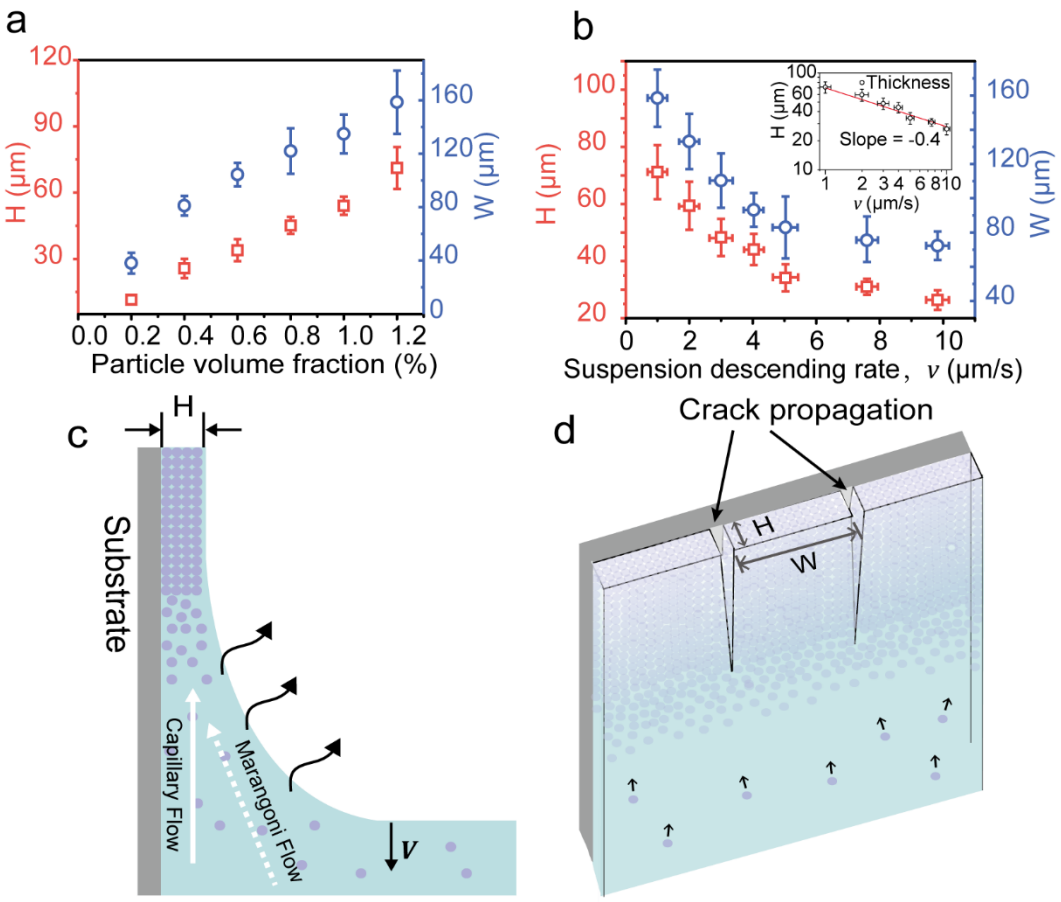

Figure 3. Optical transparency and mechanical stiffness of CRs. a) Ultraviolet-visible transmittance spectra of silica rods compared to glass slide. b) Young's modulus *E* and shear modulus *G* as a function of density of as-prepared (open symbols) and annealed (solid symbols) CRs. Inset: The density of CRs depends as a function of the annealing duration. The open square represents the density of as-prepared rods without annealing.

Max Planck Institute for Polymer Research – Author's Manuscript

For a comparison, the E and G of amorphous glass, assuming the density $\rho = 2.3\ g/cm^3$, are denoted by black and red arrows, respectively. All the dash lines in the figure are guides to the eye.

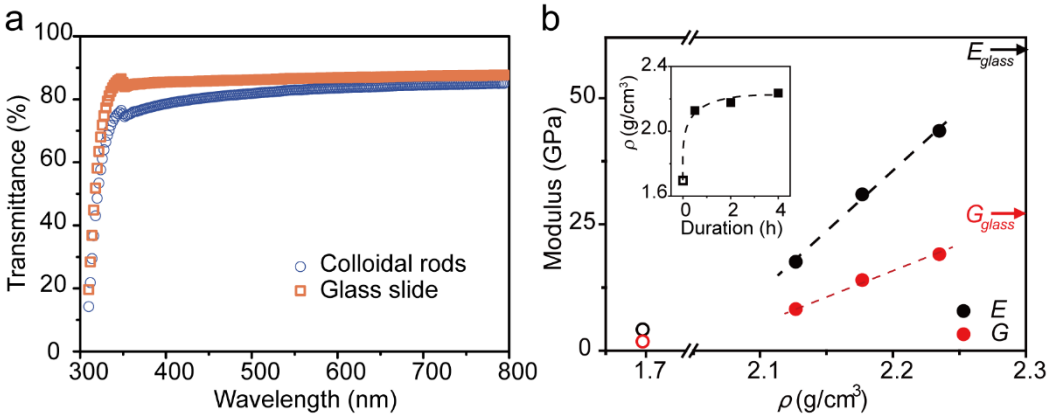

Figure 4. Effect of substrate structure on the SERS signal intensity. a) Schematic outlining the fabrication process of the Ag-coating nanostructured probe. b) SEM image of the Ag-coated nanostructured probe. c) SERS spectra obtained from 10^{-8} M BPA on different substrates.

Max Planck Institute for Polymer Research – Author's Manuscript